Article

Molecular Cell

Ribosomal Proteins Regulate MHC Class I Peptide Generation for Immunosurveillance

Graphical Abstract

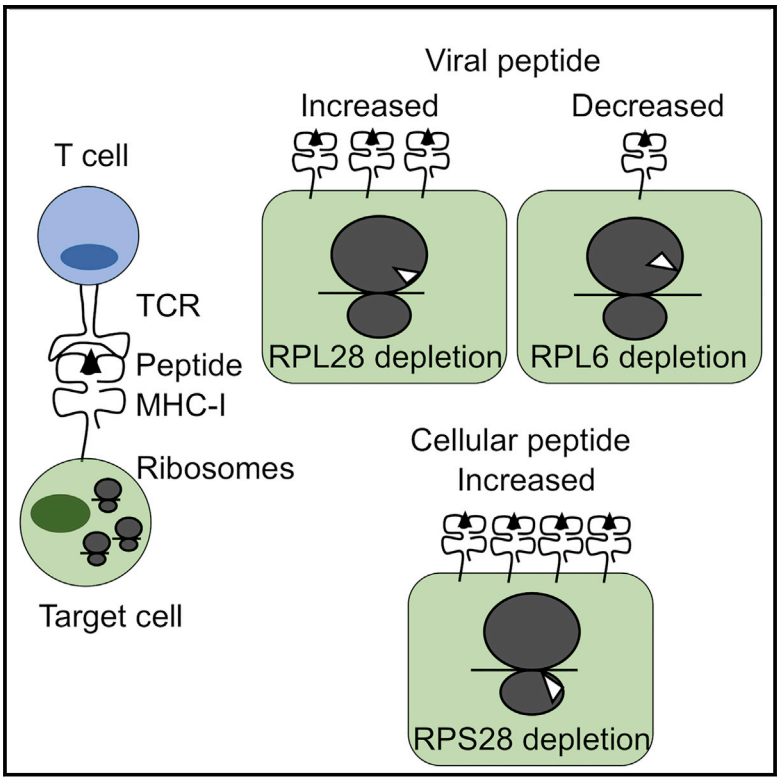

Authors

Jiajie Wei, Rigel J. Kishton, Matthew Angel, ..., Louis M. Staudt, Nicholas P. Restifo, Jonathan W. Yewdell

Correspondence

weijiajie@gmail.com (J.W.), jyewdell@niaid.nih.gov (J.W.Y.)

In Brief

Wei et al. show that cells with ribosomes lacking any one of three ribosomal protein subunits have an altered capacity to generate MHC class I peptides for immunosurveillance and that tumor cells can potentially use this mechanism to avoid CD8 T cell immunosurveillance.

Highlights

- Ribosome heterogeneity controls MHC class I peptide ligand presentation
- RPL6 and RPL28 play opposing roles in viral peptide generation
- RPS28 controls MHC class I peptide generation by modulating non-canonical translation
- Ribosomal proteins influence CD8+ T cell cancer immunosurveillance

Wei et al., 2019, Molecular Cell *73*, 1162–1173
March 21, 2019 Published by Elsevier Inc.
https://doi.org/10.1016/j.molcel.2018.12.020

CellPress

Molecular Cell
Article

Ribosomal Proteins Regulate MHC Class I Peptide Generation for Immunosurveillance

Jiajie Wei,[1,*] Rigel J. Kishton,[2] Matthew Angel,[1] Crystal S. Conn,[3] Nicole Dalla-Venezia,[4] Virginie Marcel,[4] Anne Vincent,[4] Frédéric Catez,[4] Sabrina Ferré,[5] Lilia Ayadi,[6,7] Virginie Marchand,[6,7] Devin Dersh,[1] James S. Gibbs,[1] Ivaylo P. Ivanov,[8] Nathan Fridlyand,[9] Yohann Couté,[5] Jean-Jacques Diaz,[4] Shu-Bing Qian,[3] Louis M. Staudt,[10] Nicholas P. Restifo,[2,11] and Jonathan W. Yewdell[1,12,*]

[1]Laboratory of Viral Diseases, National Institute of Allergy and Infectious Diseases, NIH, Bethesda, MD 20892, USA
[2]National Cancer Institute, NIH, Bethesda, MD 20892, USA
[3]Division of Nutritional Sciences, Cornell University, Ithaca, NY 14853, USA
[4]University of Lyon, Université Claude Bernard Lyon 1, INSERM 1052, CNRS 5286, Center Léon Bérard, Center de Recherche en Cancérologie de Lyon, Lyon, 69373 Cedex 08, France
[5]University of Grenoble Alpes, CEA, INSERM, BIG-BGE, 38000 Grenoble, France
[6]Next-Generation Sequencing Core Facility, UMS2008 IBSLor CNRS-INSERM-University of Lorraine, 54505 Vandoeuvre-les-Nancy, France
[7]Laboratory IMoPA, UMR7365 CNRS-University of Lorraine, 54505 Vandoeuvre-les-Nancy, France
[8]Laboratory of Gene Regulation and Development, Eunice Kennedy Shriver National Institute of Child Health and Human Development, NIH, Bethesda, MD 20892, USA
[9]Laboratory of Translational Biology, School of Biosciences and Biotechnology, University of Camerino, Camerino MC 62032, Italy
[10]Lymphoid Malignancies Branch, National Cancer Institute, NIH, Bethesda, MD 20892, USA
[11]Center for Cell-Based Therapy, Center for Cancer Research, NIH, Bethesda, MD 20892, USA
[12]Lead Contact
*Correspondence: weijiajie@gmail.com (J.W.), jyewdell@niaid.nih.gov (J.W.Y.)
https://doi.org/10.1016/j.molcel.2018.12.020

SUMMARY

The MHC class I antigen presentation system enables T cell immunosurveillance of cancers and viruses. A substantial fraction of the immunopeptidome derives from rapidly degraded nascent polypeptides (DRiPs). By knocking down each of the 80 ribosomal proteins, we identified proteins that modulate peptide generation without altering source protein expression. We show that 60S ribosomal proteins L6 (RPL6) and RPL28, which are adjacent on the ribosome, play opposite roles in generating an influenza A virus-encoded peptide. Depleting RPL6 decreases ubiquitin-dependent peptide presentation, whereas depleting RPL28 increases ubiquitin-dependent and -independent peptide presentation. 40S ribosomal protein S28 (RPS28) knockdown increases total peptide supply in uninfected cells by increasing DRiP synthesis from non-canonical translation of "untranslated" regions and non-AUG start codons and sensitizes tumor cells for T cell targeting. Our findings raise the possibility of modulating immunosurveillance by pharmaceutical targeting ribosomes.

INTRODUCTION

By displaying oligopeptides on the cell surface, major histocompatibility complex class I (MHC class I) molecules enable T cell immunosurveillance of viruses and other intracellular pathogens, cancers, transplants, and autoimmune targets and mediate additional functions, including natural killer (NK) cell activation, mate selection, hormone receptor function, and neuronal development.

MHC class I antigenic peptides typically arise from proteasomal products transported by TAP (transporter associated with antigen processing) into the endoplasmic reticulum (ER), trimmed at their NH_2 termini, loaded onto class I molecules, and transported to the cell surface. Such endogenous MHC class I peptide ligands have two potential sources: "retirees" and "DRiPs" (defective ribosomal products). Retirees are proteins that attain stable structures and exhibit normal turnover kinetics, i.e., a median half-life of 46 h across the entire proteome (Schwanhäusser et al., 2011). The rapid presentation of peptides from otherwise highly stable viral proteins prompted the DRiP hypothesis that peptides arise from translation products that cannot or do not achieve a stable structure and are rapidly degraded (Antón and Yewdell, 2014; Yewdell et al., 1996).

DRiPs include translation products resulting from inevitable errors in transcription, translation, folding, targeting, and assembly. An important class of DRiPs arise from non-canonical translation, including CUG codon initiation (Starck et al., 2012), downstream initiation (Berglund et al., 2007), alternative reading frame translation (Bullock and Eisenlohr, 1996), intron translation (Apcher et al., 2013; Coulie et al., 1995), and nuclear translation (Apcher et al., 2013; Dolan et al., 2010a).

DRiPs have a central role in peptide generation for viral and tumor immunosurveillance. Viral peptide class I complexes can be detected even prior to detection of viral proteins (Croft et al., 2013; Esquivel et al., 1992). Rapid presentation of antigenic peptides enables CD8+ T cells to recognize and kill virus-infected

cells before progeny virions can be released. In the context of tumor immunosurveillance, a positive correlation between checkpoint inhibitor efficacy in immunotherapy and the number of somatic mutations present in tumor cells implicates mutated self-peptides as important targets of tumor-specific T cell. Given the increased tendency for mutant proteins to misfold, this supports a role for DRiPs in neoantigen presentation.

The close association between DRiP translation and peptide generation raises the possibility of specialization in the translation apparatus in antigen presentation. Shastri and colleagues have shown that translation of CUG-initiated antigenic peptides relies on non-canonical translation initiation and a dedicated initiator Leu-tRNA (Starck and Shastri, 2016). Ribosomes can potentially exhibit enormous heterogeneity, and myriad varieties of modifications have been discovered on both ribosomal RNAs and proteins (Erales et al., 2017; Higgins et al., 2015). Numerous reports that ribosomes lacking one or more of their 80 proteins can exhibit distinct functions (Dinman, 2016; Shi and Barna, 2015; Shi et al., 2017) are consistent with the idea that specialized ribosomes (i.e., ''immunoribosomes''; Yewdell and Nicchitta, 2006) preferentially synthesize DRiPs for immunosurveillance.

Here, we show that ribosomes lacking one of three identified protein subunits demonstrate altered efficiencies in generating peptides. This establishes that ribosome modifications can selectively modulate the generation of DRiP derived antigenic peptides and raises the possibility of therapeutically manipulating DRiP translation to modulate immunosurveillance of pathogens, tumors, and autoantigens.

RESULTS

RPs Regulate MHC Class I Peptide Presentation

To examine the role that individual ribosomal proteins (RPs) play in MHC class I peptide generation we constructed a lentiviral short hairpin RNA (shRNA) panel that targets each of the 80 RPs (Table S1). We then tested each virus for its ability to modulate MHC class I peptide presentation in HEK293-K^b cells (HEK293 cells expressing the mouse class I molecule H-$2K^b$ from a transgene), allowing 6–7 days to reduce levels of RPs via cell division and normal RP turnover following shRNA-mediated shutdown of RP synthesis (Figure 1A).

We measured cell-surface MHC class I expression by flow cytometry using a panel of four monoclonal antibodies (mAbs) that bind either: 1) the β_2-microglobulin (β2 m) subunit, 2) all human classical class I molecules, 3) histocompatibility leukocyte antigen (HLA)-A2 (endogenous to HEK293 cells) or, 4) K^b (Figure 1A). We also used the 25-D1.16 mAb to measure K^b molecules bound to the model peptide SIINFEKL generated after infecting cells with a recombinant influenza A virus (rIAV) encoding SIINFEKL in the stalk of the NA glycoprotein (rIAV-NA-SIINFEKL). Simutaneously staining cells with a NA-specific mAb, we could determine the ratio of K^b-SIINFEKL to its source protein in order to control for RP knockdown effects on IAV gene expression (Figure 1A). Red fluorescent protein (RFP) expression by the lentiviral shRNA vector enabled gating on non-transduced cells (RFP−) as an internal standard to detect subtle changes in class I expression and to control for IAV infection dose in cells with unaltered ribosomes (Figure 1B).

As an example of raw data acquisition and quantification, in the case of RPS6 (eS6) knockdown, staining with each Ab is reduced in transduced cells (Figures 1C and 1D, quantification given in Figure 1E). Importantly, NA and K^b-SIINFEKL signals are equally diminished, resulting in no change in peptide generation per NA molecule synthesized (Figure 1C, bottom panel, and quantification given in Figure 1E, upper panel). This is typical of knockdown of many RPs, which are expected to reduce overall protein synthesis due to reduced numbers of functional ribosomes (Figure 1F). Notably, RPS4Y1 knockdown had little effect on NA or class I expression, consistent with the absence of this Y-chromosome-encoded RP in a cell line derived from a female donor (Figure S1).

Strikingly, both 60S ribosome subunit and 40S ribosome subunit contain RPs (respectively, RPLs and RPSs) that specifically modulate MHC class I peptide cell-surface expression. RPS10, RPS13, RPS28, RPLP0, RPLP1, and RPL3 selectively regulate cell-surface human class I molecules, including HLA-A2, having no or the opposite effect on H-$2K^b$ (Figure 1F, highlighted by unfilled arrows). RPS7, RPS15A, RPL6, RPL17, RPL28, RPL38, RPL39, and RPL40 regulate K^b-SIINFEKL generation without affecting viral protein translation (Figure 1F, highlighted by filled arrows.)

RP Knockdown Has Minor Effects on Transcriptome

As protein translation is exquisitely sensed by cellular pathways that can modulate various aspects of MHC class I biogenesis, it was essential to assess how individual RP knockdown alters general cell functions. Selecting the RPs with most pronounced effects on class I expression or class I viral peptide complex generation, while not affecting overall translation (RPLP0, RPL3, RPL6, RPL28, and RPS28), we performed microarray analysis to determine the effects of RP knockdown on the transcriptome.

Cluster analysis based on 35,211 microarray probes revealed that of the five RPs examined, RPL28 (eL28), RPS28 (eS28), and RPL6 (eL6) knockdowns most resembled scrambled control transduced cells (shControl) (Figure 2A; GEO: GSE114484). RPL3 and RPLP0 perturbed the transcriptome more dramatically, suggesting these two RPs could affect class I expression by altering multiple intertwined cellular pathways. As a result, we focused on RPL28, RPS28, and RPL6 in the following studies. Importantly, differences between each of these RP knockdowns and shControls are similar in magnitude to differences between the two different shControls, demonstrating that they only have minor effects on the transcriptome (Figures 2B and 2C). Only a small number of transcripts demonstrate significant changes ($p < 0.05$), with few exhibiting larger than a 2-fold change compared to shControl1 and shControl2 (colored red in Figure 2C). Even with RPL6 knockdown, which exhibits the greatest difference from shControls, alterations in the transcriptome are minor, with RPL6 mRNA level itself being most severely affected (~4-fold decrease) (Figure 2C). For RPL28 and RPS28, in addition to the RP mRNAs, the corresponding pseudogene mRNAs lacking protein-coding ability are also changed, likely due to the presence of shRNA targeting sequence in the transcripts.

Remarkably, given the possibility of coordinated RP mRNA regulation, other RP mRNAs exhibited only minor changes in abundance (Figure S2), with the exception that RPL13A mRNA

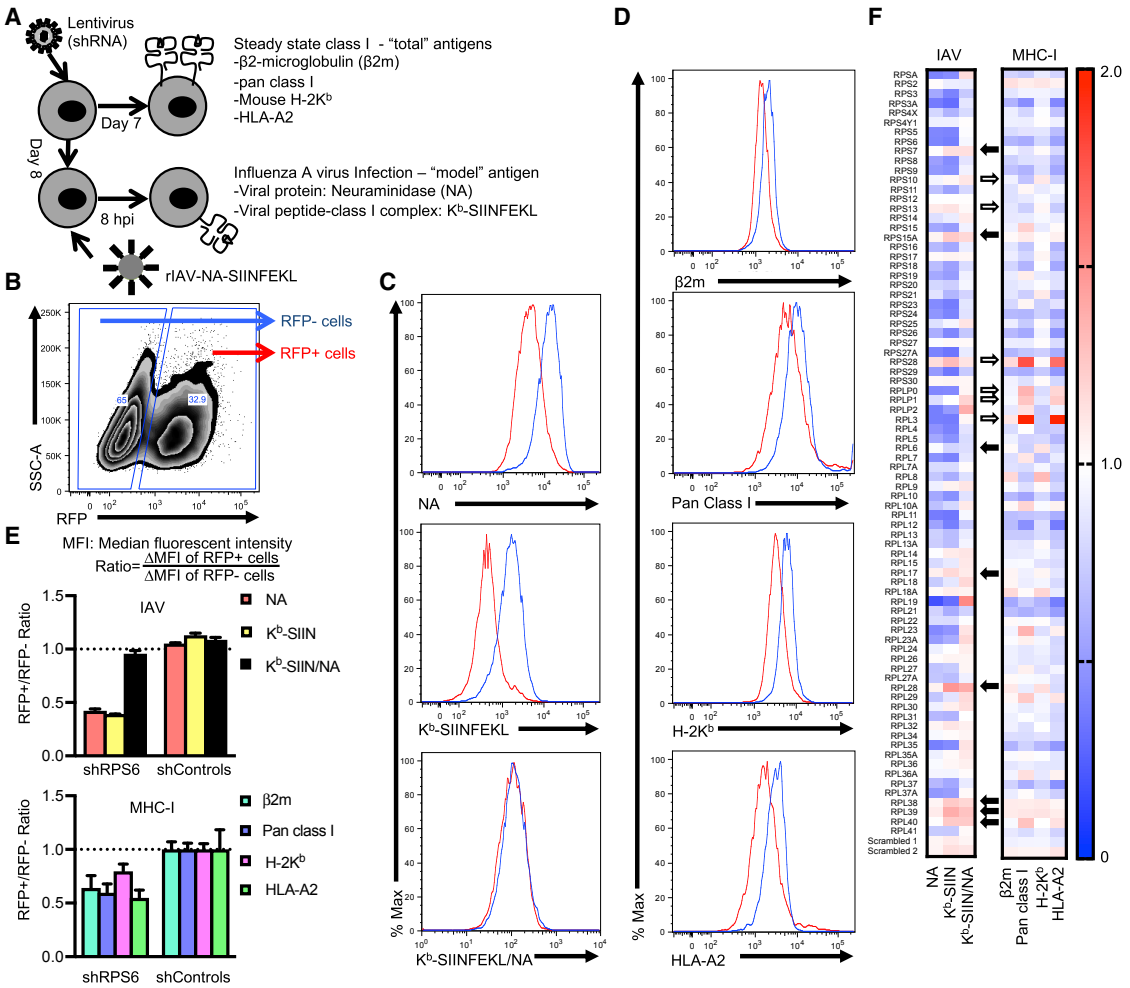

Figure 1. RPs Show Differential Effects on MHC Class I Antigen Presentation

(A) Schematic representative of experimental design. Levels of indicated cell-surface proteins were measured after lentiviral transduction by flow cytometry.

(B–D) Representative flow cytometry analysis. HEK293-K^b cells infected with shRNA lentivirus gated by side scatter area (SSC-A) and red fluorescent signal (RFP) (B). Transduced cells (RFP+, red) in (C) and (D) were compared to non-transduced cells (RFP−, blue) in (C) and (D). (C) Expression levels of NA (upper), K^b-SIINFEKL (middle), and the ratio of K^b-SIINFEKL to NA (bottom) on individual RFP+ cells (in red) and RFP− cells (in blue). The ratio was multiplied by 1,000 to scale the value. Expression levels of β2 m, pan class I, H-2K^b, and HLA-A2 on individual RFP+ cells (in red) and RFP− cells (in blue) (D).

(E) Median fluorescent intensity over background (ΔMFI) of RFP+ cells compared with that of RFP− cells to quantify the effect of knocking down individual RPs like in (C) (upper) and (D) (bottom). Center values and error bars represent mean ± range (n = 2 independent experiments).

(F) Heatmap showing the effects of knocking down individual RPs on MHC class I surface expression (right) and viral protein expression and peptide generation (left) (n = 2 independent experiments). Filled arrows indicate RPs with selective effects on viral peptide generation. Unfilled arrows indicate RPs with selective effects on MHC class I surface expression.

See also Figure S1.

was also decreased 2-fold in RPS28 knockdown cells (Figure S2). Because RPL13A knockdown does not recapitulate the RPS28 knockdown phenotype (Figure S1), it is unlikely to contribute to the effect of RPS28 shRNA antigen presentation (Figure S1).

Gene ontology (GO) term analysis of all the significantly changed transcripts ($p < 0.05$) in either comparison to shControl1 or shControl2 cells revealed different patterns among three knockdown cells (Figure 2D). For RPL28 knockdown, only "nucleosome-assembly"-associated mRNAs achieved significance ($p < 0.001$). By contrast, nine mRNA families were significantly altered in RPL6 knockdown cells, with three related to protein translation. For RPS28, 4 of 10 altered families were translation related. Importantly, none of the three knockdowns altered "antigen presentation"-related mRNAs, and at the individual gene level, knocking down RPL6, RPL28, or RPS28 does not significantly alter mRNA levels of known genes associated with MHC class I antigen processing, or the p53 pathway as a result of ribosome biogenesis stress. These data indicated that knocking down RPS28, RPL6, and RPL28 has a minor effect on the transcriptome and therefore likely regulates class I peptide presentation through mechanisms independent of regulating individual mRNA transcripts.

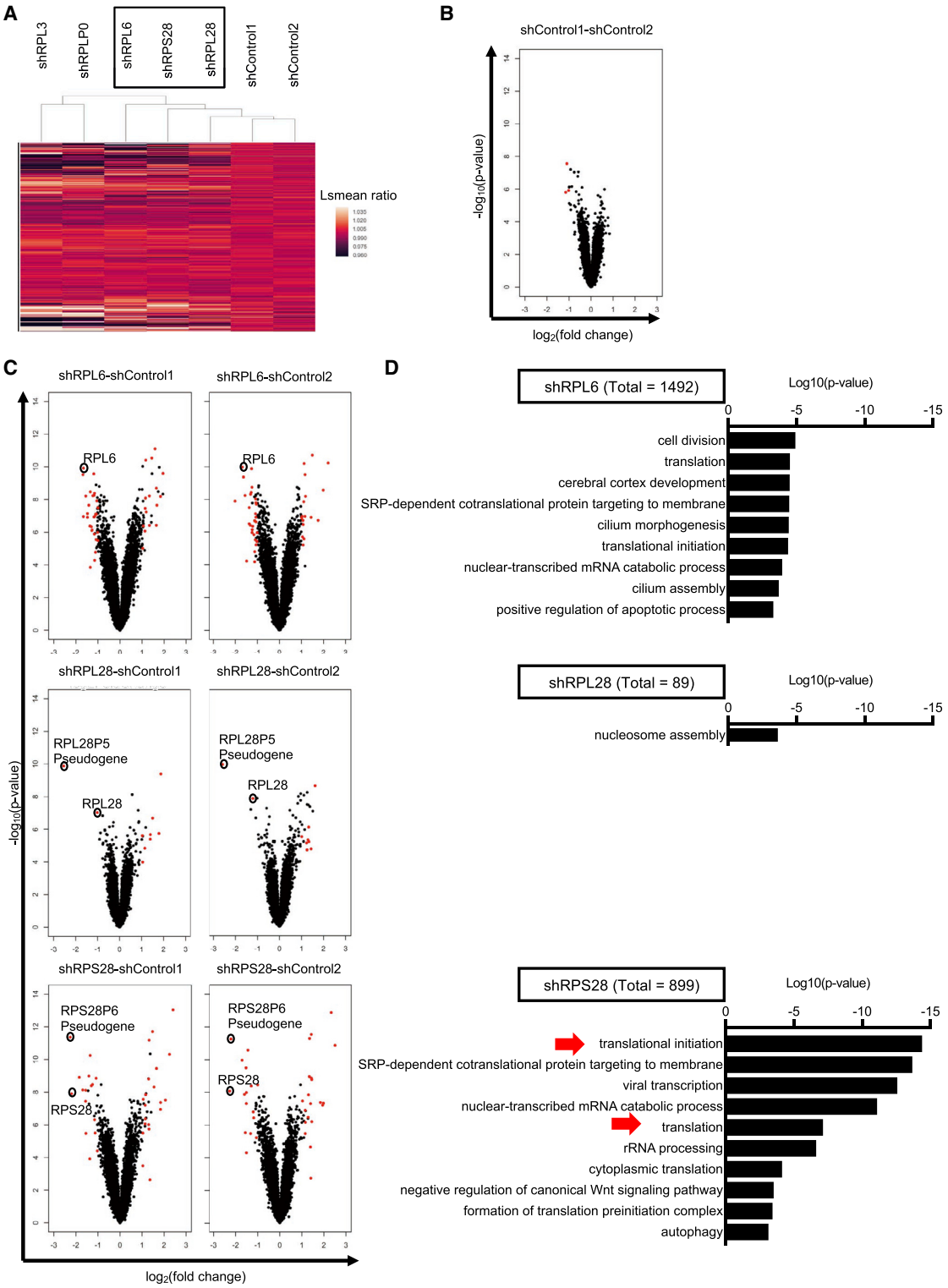

Figure 2. RP Knockdown Has Minor Effects on the Transcriptome

(A) Heatmap and hierarchical clustering showing the effect of knocking down indicated RP genes on 35,211 probes in microarray. Least-squares means (lsmeans) of each knockdown is compared with the average of lsmeans of two shControls.

(B) Volcano plots comparing two shControls. Probes with adjusted p values < 0.05 and absolute $\log_2$ (fold change) > 1 are colored red.

(legend continued on next page)

RP Knockdown Has Minor Effects on Ribosome Protein Content

To further characterize the potential cascading effects of RP knockdown, we used a mass spectrometry (MS)-based quantitative proteomic approach to analyze the protein content of ribosomes purified from RPL28 knockdown versus shControl cells (Erales et al., 2017) (Figure 3A). Of 80 reproducibly quantified RPs and a number of associated proteins, only RPL28 (~7-fold reduction) and 8 non-RPs show a strongly significant change. Of 8 non-RPs, 5 proteins have RNA-based functions, including translation initiation (eIF3D), mRNA cap formation (RNGTT), RNA metabolism (IMPDH2), and putative RNA binding (MAK16 and C7orf50), whereas 3 proteins are not known to be involved in translation (RPS6KC1, DNAH8 and STON2).

RiboMethSeq analysis reveals that RPL28 depletion modulated the methylation status of three 28S rRNA sites (Am2388, Gm4588, and Gm4607) (Figure 3B). These findings show that reduction in a single RP alters ribosomes by changing methylation patterns and modulating associated proteins, without necessarily altering other RPs.

To summarize, using a lentiviral panel to knock down each RP, we identified three RP knockdowns for further characterization—RPL6, RPL28, and RPS28—that regulate MHC class I antigenic peptide generation yet have minor effects on the transcriptome. We also show that RP knockdown can potentially alter ribosome function by inducing changes in ribosome associated proteins and rRNA methylation patterns.

Opposite Roles of RPL6 and RPL28 in Peptide Generation

Eight hours post-infection with rIAV-NA-SIINFEKL, RPL6 knockdown decreased cell-surface K^b-SIINFEKL while RPL28 knockdown had the opposite effect (Figure 4A, left panel), despite neither knockdown affecting NA cell-surface expression. To rule out the possibility that modulation of K^b-SIINFEKL surface expression by RPL6 and RPL28 results from altering β_2m or K^b levels, we measured the total cell-associated K^b by immunoblotting (Figure S3A) and surface expression of β_2m and K^b by flow cytometry (Figure S3B). Neither RPL6 nor RPL28 knockdown significantly changed β_2m cell-surface expression or total cell-associated immunoblotted K^b. The slight increase of surface H-2K^b (1.2-fold) on RPL28 knockdown cell surface cannot account for the 2-fold increase in K^b-SIINFEKL (Figure 4A). We reasoned that RPL6 and RPL28 changed the supply of SIINFEKL to be loaded onto K^b in the ER.

SIINFEKL generation from IAV-encoded NA is proteasome/Ub dependent (Dolan et al., 2010b; Wei et al., 2017), so we next examined presentation of SIINFEKL appended to the COOH terminus of the IAV M2 membrane protein, which is both proteasome and Ub independent (Yang et al., 2016). M2 cell-surface expression was not altered by RPL6 knockdown, while we typically observed a 10% decrease by RPL28 depletion. Despite the slight decrease in M2 expression, RPL28 depletion increased K^b-SIINFEKL generation, resulting in a ~2-fold increase in the complex to source protein ratio. Remarkably, RPL6 had no significant effect on K^b-SIINFEKL generation (Figure 4A, right panel), indicating that RPL6's impact on antigen presentation is peptide context dependent, providing further evidence that is not due to global alterations in K^b expression or trafficking.

To more precisely assess peptide presentation, we performed kinetic analysis following infection with rIAVs (Figure 4B). Consistent with SIINFEKL generation from DRiPs, K^b-SIINFEKL cell expression kinetics nearly perfectly paralleled surface expression of NA and M2, despite their high metabolic stabilities (Dolan et al., 2010b; Yang et al., 2016). Neither NA nor M2 cell-surface expression was significantly affected by RPL6 or RPL28 knockdown (Figure 4B, right panel). Recapitulating the single time point experiments, RPL28 knockdown cells showed a dramatic enhancement of K^b-SIINFEKL regardless of the source protein (used to normalize the relative K^b-SIINFEKL expression of each infected cell), while K^b-SIIFNEKL inhibition by RPL6 was dependent on the SIINFEKL context in its IAV fusion protein (Figure 4B, left panel).

Next, we examined K^b-SIINFEKL generation in four different IAV-encoded contexts (Figures 4C and S3C). In each case, RPL28 depletion increases K^b-SIINFEKL presentation. By contrast, RPL6 knockdown has no effect on ER-targeted (ES) or cytosolic (Ub) SIINFEKL, while decreasing presentation of SIINFEKL that must be liberated from NS1 or M2. Using a cell permeant Ub-E1-activating enzyme inhibitor, MLN7243 (Wei et al., 2017), we found that RPL6 knockdown inhibition of SIINFEKL presentation parallels E1 dependence of peptide generation (Figure 4D). Although MLN7243 nearly abolished K^b-SIINFEKL expression from NA, NS1, and M2(45), it had little effect on presentation from M2(C-term), Ub-, or ER leader sequence-fusion proteins appended to PB1 (results summarized in Figure S3C).

Since RPL6 selectively affects Ub/proteasome-dependent SIINFEKL generation from DRiPs, and DRiPs provide a substantial fraction of ubiquitylated proteins (Kim et al., 2011; Schubert et al., 2000; Wang et al., 2013), we examined whether RPL6 depletion affected the overall ubiquitylated protein pool. Immunoblotting with the FK2 mAb, specific for poly- and mono-ubiquitylated proteins revealed a modest (15%–30%) but reproducible increase in the smear of high molecular weight polyubiquitylated proteins that are substrates of proteasomes, without altering discretely ubiquitylated individual species. A species with a molecular weight corresponding to monoubiquitylated H2A serves as an internal control for extraction and loading (Figure 4E). Given the RPL6 blockade in Ub-dependent SIINFEKL presentation, this finding is consistent with the idea that RPL6 knockdown interferes with ubiquitin-proteasome mediated degradation of DRiPs.

(C) Volcano plots comparing RPs knockdown with two shControls. Probes with adjusted p values < 0.05 and absolute $\log_2$ (fold change) > 1 in both comparisons are colored red (n = 2 biological replicates).

(D) Significantly different transcripts revealed by microarray were segregated by Visualization and Integrated Discovery (DAVID) v6.8 for Gene Ontology (GO) terms enrichment (n = 2 biological replicates).

Statistical analyses were performed as described in STAR Methods: RNA purification and microarray analysis. See also Figure S2.

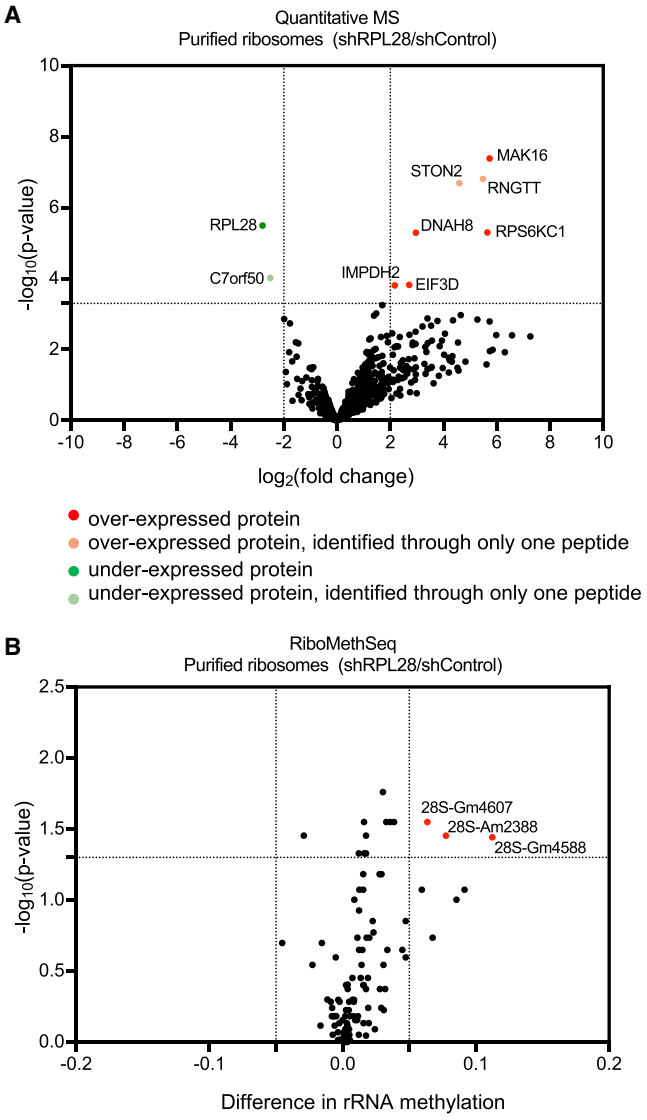

Figure 3. RP Knockdown Has Minor Effects on Ribosome Protein Content

(A) Quantitative MS-based proteomic analysis comparing protein contents of control ribosomes with RPL28 knockdown ribosomes. All quantified proteins were plotted. Significant changed sites are labeled. Dotted lines indicate $p < 0.005$ and abs [$\log_2$ (fold change)] > 2.

(B) RiboMethSeq assay measuring rRNA methylation status comparing control ribosomes with RPL28 knockdown ribosomes. Dotted lines indicate $p < 0.05$ and abs (difference) > 0.05. Significant changed sites (Am2388, Gm4588, and Gm4607 found in 28S rRNA) are colored in red (n = 5 technical replicates). Statistical analyses were performed as described in STAR Methods: Proteomics, RiboMethSeq and statistical analysis.

Taken together, we show that RPL6 and RPL28 have opposite roles in modulating peptide generation. RPL6 knockdown selectively inhibits Ub-dependent peptide generation implicating RPL6 in degrading DRiP substrates, while RPL28 knockdown enhances SIINFEKL presentation in all circumstances (TAP/ubiquitin/proteasome dependent/independent). Intriguingly, RPL6 and RPL28 are located in close proximity within the ribosome (Figure 4F), with a number of contact residues, identifying this ribosome domain as having a specific role in class I peptide generation.

RPS28 Controls Non-canonical Translation and Influences Tumor Immunosurveillance

40S small ribosomal subunit protein S28 (RPS28) knockdown cells increase cell-surface expression of HLA-A2, and perhaps other human class I molecules recognized by pan class I Ab W6/32 (Figure 5A). It does not, however, increase K^b surface expression (Figures 1 and S1), indicating that the HLA-A2 increase is unlikely to be due to increases in expression of proteins involved in antigen processing. Consistent with this conclusion, HLA-A2 upregulation persists in RPS28 knockdown cells after increasing expression of processing components by treating cells for 24 h with interferon (IFN)-γ (Figure 5A). Further, RPS28 knockdown does not increase expression of TAP (Figure 5B), whose levels are typically regulated in parallel with other antigen processing pathway components. The slight upregulation of total MHC class I level (~1.2-fold; Figure 5B) cannot account for the 2-fold change of surface class I. Rather, in RPS28 knockdown cells, cell-surface HLA-A2 recovers more rapidly from acid-mediated removal of native HLA-A2 cell surface molecules, consistent with increased peptide generation (Figure 5C).

To determine the extent to which RPS28 control of antigen generation is limited to TAP-dependent peptides, we stably expressed in HEK293-K^b cells the potent TAP inhibitor ICP47 (Hill et al., 1995) (Figure 5D). As expected, ICP47 expression reduced cell-surface HLA-A2 levels (Figure 5D, middle). HLA-A2 upregulation persisted in RPS28 knockdown HEK293-K^b cells containing ICP47, though at a slightly diminished level (Figure 5D, right). This indicates that RPS28 affects both TAP-dependent and -independent peptide generation.

Gene ontology enrichment analysis of the transcriptome alterations in RPS28 knockdown cells identifies "translational initiation" and "translation" in the top 5 categories with strong significance (Figure 2D). Based on this and findings that RPS28 locates in the "accuracy center" of the ribosome (Alksne et al., 1993) and modulates start codon usage in yeast (Anthony and Liebman, 1995) we hypothesized that RPS28 knockdown increases peptide generation by increasing non-canonical translation.

To test this, we employed ribosome profiling (Ribo-Seq) to characterize the effect of RPS28 knockdown on the translatome (Ingolia et al., 2011). For both shControl and RPS28 knockdown cells, we observed strong correlation between biological replicates (Figure S4A). As expected, RPS28 expression itself is downregulated, as demonstrated by reduced reads in the protein-coding region (Figure S4B). Consistent with microarray analysis (Figure 2), RNA sequencing (RNA-seq) performed simultaneously with Ribo-Seq revealed a high correlation (r = 0.9131) between control and knockdown cells at the mRNA level (Figure S5A, left panel). The Ribo-Seq correlation is weaker (r = 0.8937) (Figure S5A, right panel), consistent with a role for RPS28 in translational regulation. Indeed, by calculating translation efficiencies (the ratio between Ribo-Seq RPKM and RNA-seq RPKM), we observed that RPS28 knockdown mainly selectively downregulates translation of a relatively small mRNA subset (Figure 6A).

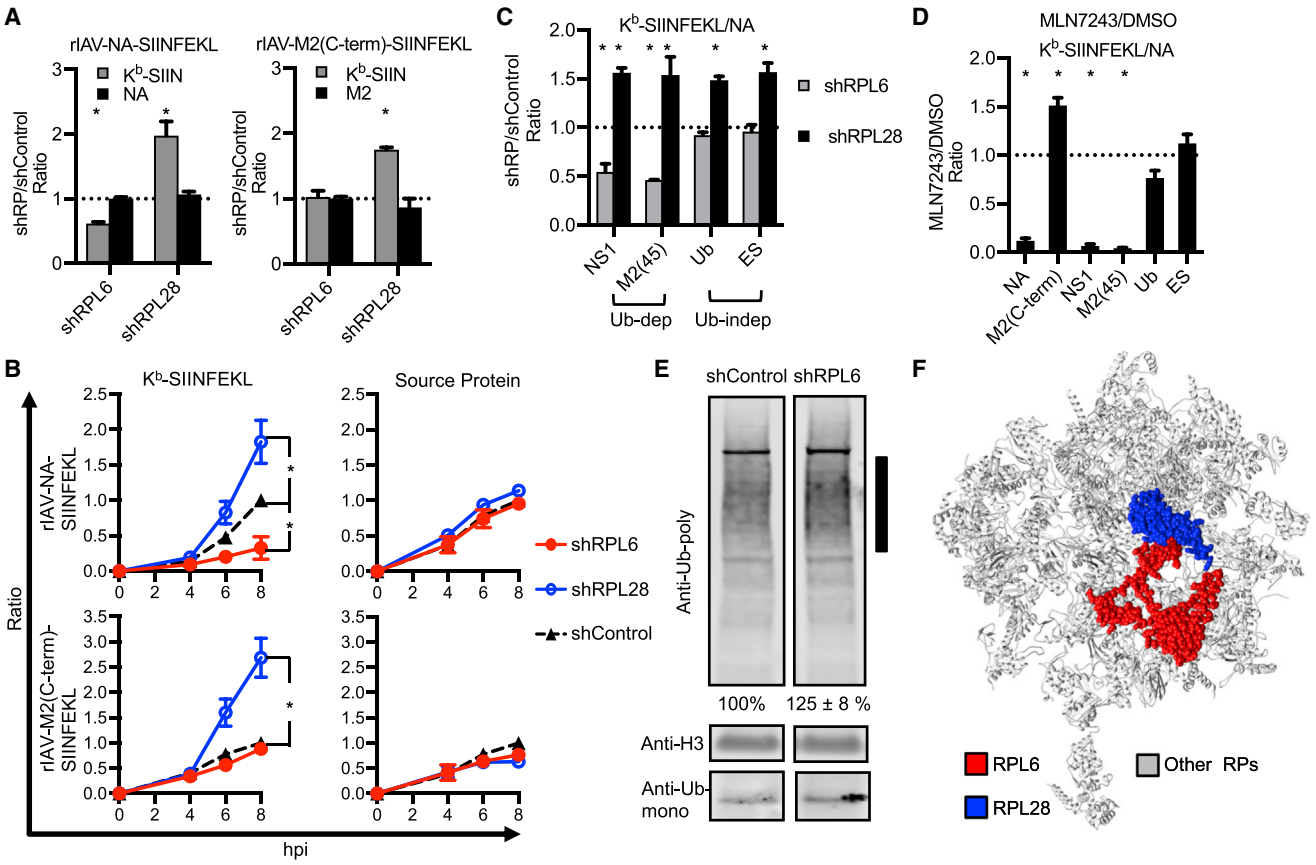

Figure 4. RPL6 and RPL28 Modulate K^b-SIINFEKL Generation

(A) Source protein and K^b-SIINFEKL expression levels on cells infected with IAV encoding SIINFEKL in NA (left) or M2 (right) genes at 8 h post-infection (hpi). Results are normalized first to internal non-transduced control cells and then to shControls.

(B) Kinetics of K^b-SIINFEKL (left) and source protein (NA or M2, right) expression after IAV infection. MFI of each time point was normalized to that of shControl at 8 hpi.

(C) K^b-SIINFEKL generation from indicated rIAVs in knockdown cells.

(D) K^b-SIINFEKL generation from indicated rIAVs in response to the E1 inhibitor MLN7243.

(E) Immunoblotting of RPL6 knockdown cells and shControl cells. Black bar indicates the region used for quantification. Values represent mean ± range after normalizing to loading control histone H3 (n = 3 independent experiments). *$p < 0.05$ with a one-sample t test.

(F) Ribosome structure adapted from human 80S ribosome (PDB:4V6X) with rRNA hidden (generated by Chimera[37]).In (A)–(D), all values are mean ± SEM. (n = 4 independent experiments). In (A), (C), and (D), *$p < 0.05$ by two-tailed one-sample t test. In (B), *$p < 0.05$ by two-way ANOVA.

See also Figure S3.

Importantly, Ribo-Seq showed that RPS28 knockdown cells contain a higher fraction of reads in both 5′ UTR and 3′ UTR, demonstrating that RPS28 knockdown increases non-canonical translation by enhancing translation from these "untranslated regions." The UTR derived-read fraction was not altered in the RNA-seq (Figure 6B, right panel), indicating RPS28 modulates UTR translation per se and not UTR-containing mRNA. In addition, codon usage analysis revealed that, although the hierarchy of codon usage was similar to control cells, RPS28 knockdown cells increased non-AUG codon initiation (Figure 6C), further perturbing the translatome.

We confirmed that RPS28 knockdown enhances non-canonical translation by plasmid driven reporter assays (Figure 6D). We observed increased translation of both GFP with an internal ribosome entry site (IRES) leader relative to cap-dependent translation of BFP, and CUG initiated GFP relative to AUG initiated BFP. Taken together, we conclude that RPS28 knockdown is likely to increase class I expression by increasing non-canonical translation of peptide generating-DRiPs.

A recent study reported that RPs are selectively enriched in a genome-wide CRISPR/Cas9 survey to identify genes involved in tumor escape from CD8+ T cell-mediated killing (Patel et al., 2017). To examine the contribution of RPS28 to T cells immunosurveillance, we tested the effect of RPS28 knockdown on killing of human melanoma cells by HLA-A2-restricted, NY-ESO-1-specific T cells (Figure 6E). Lentivirus-mediated RPS28 knockdown in Mel624 cells increased T cell killing, consistent with increased presentation of the NY-ESO-1 peptide-A2 complex and the conclusion that ribosome-based modulation of CD8+ T immunosurveillance facilitates tumor cell immunoevasion. Since

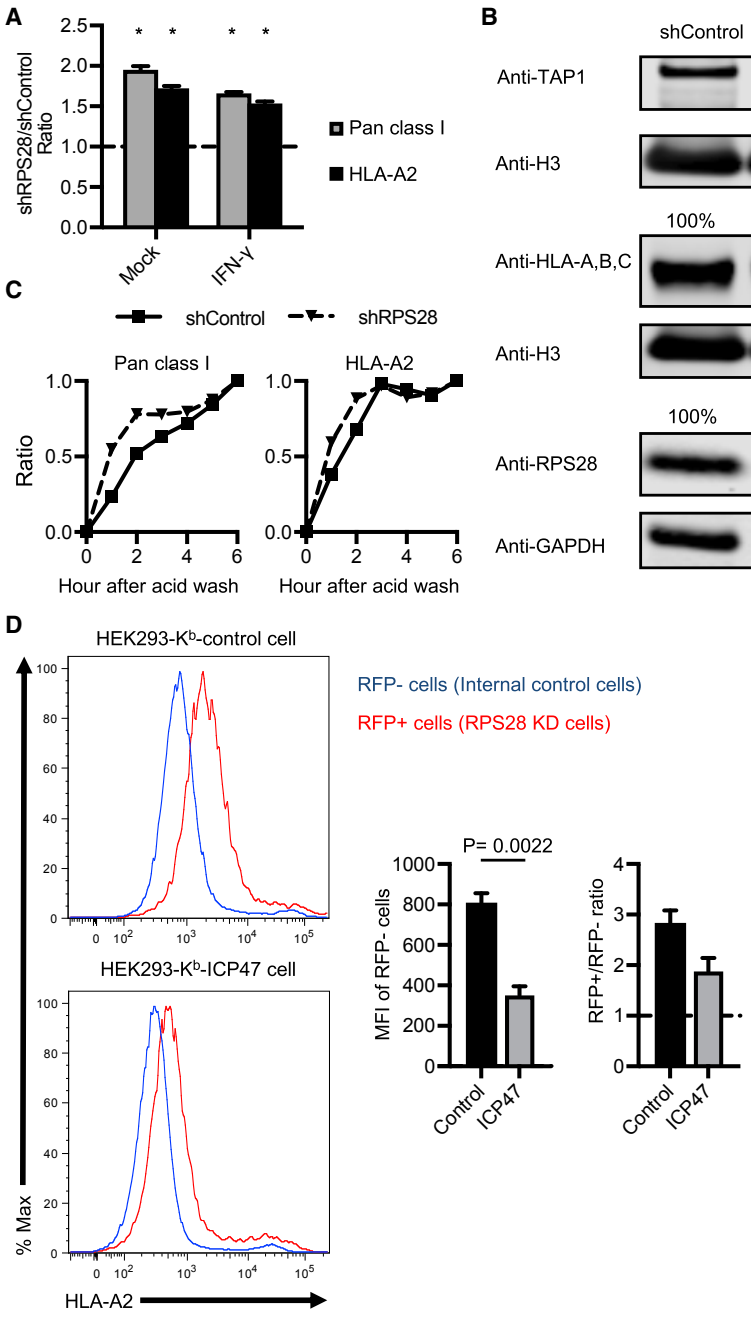

Figure 5. RPS28 Regulates Cell-Surface MHC Class I Expression

(A) Pan class I and HLA-A2 levels in response to IFN-γ. *p < 0.05 by a two-tailed one-sample t test (n = 3 independent experiments).

(B) Immunoblotting of RPS28 knockdown cells and shControl cells. Values represent mean ± range after normalizing to loading control (n = 3 biological replicates).

(C) Recovery kinetics of pan class I and HLA-A2 after acid wash. For each sample, increased MFI after acid wash at indicated time points was normalized to the last time point. Data representative of three independent experiments.

(D) Flow cytometry analysis comparing HEK293-K^b cells with and without ICP47. Left: representative histograms. Middle: MFI of non-transduced cells was compared to evaluate the level of HLA-A2 on cells with and without ICP47. Statistical significance was evaluated with a two-tailed unpaired t test. Right: RPS28 knockdown cells (RFP+) were compared with non-transduced cells (RFP−) to quantify the effect of RPS28 knockdown. Center values and error bars represent mean ± SEM (n = 3 biological replicates).

somatically acquired RP mutations are extremely common in human cancer (Ajore et al., 2017; Kandoth et al., 2013), our findings suggest the potential for modulating ribosome functions pharmaceutically or genetically to enhance cancer immunotherapy.

DISCUSSION

Our findings extend prior observations that cells can function with significant fractions of ribosomes lacking certain individual RPs, and that the effects of RP absence can vary between cell or tissue types with highly selective effects on translating individual mRNAs (Briggs and Dinman, 2017; Shi and Barna, 2015; Shi et al., 2017; Xue and Barna, 2012; Lee et al., 2013). Most importantly, we establish the principle that peptide generation for immunosurveillance can be controlled by intrinsic alterations to ribosomes themselves, in addition to exploiting extrinsic translation factors, as has been amply demonstrated (Apcher et al., 2011, 2013; Dolan et al., 2010a; Prasad et al., 2016; Schmidt, 2009; Starck et al., 2012). Whether intrinsic ribosomal alterations are naturally exploited to positively or negatively influence MHC class I immunosurveillance of foreign and self-antigens remains to be established, though it seems likely, particularly in cancer immunoediting. At a minimum, our findings show that alterations in ribosomes can change the efficiency of class I peptide presentation independently of their effects on the amount of native source proteins translated.

Detailed characterization of ribosomes from RPL28 knockdown cells provides a clear demonstration that modifying individual RPs can, without changing other RPs, alter rRNA methylation and increase/decrease extrinsic translation factors that stably associate with ribosomes. RPL28 increases presentation of the SIINFEKL model peptide from all IAV encoded translation products, including TAP- and Ub-independent antigens, consistent with physically or functionally (via molecular

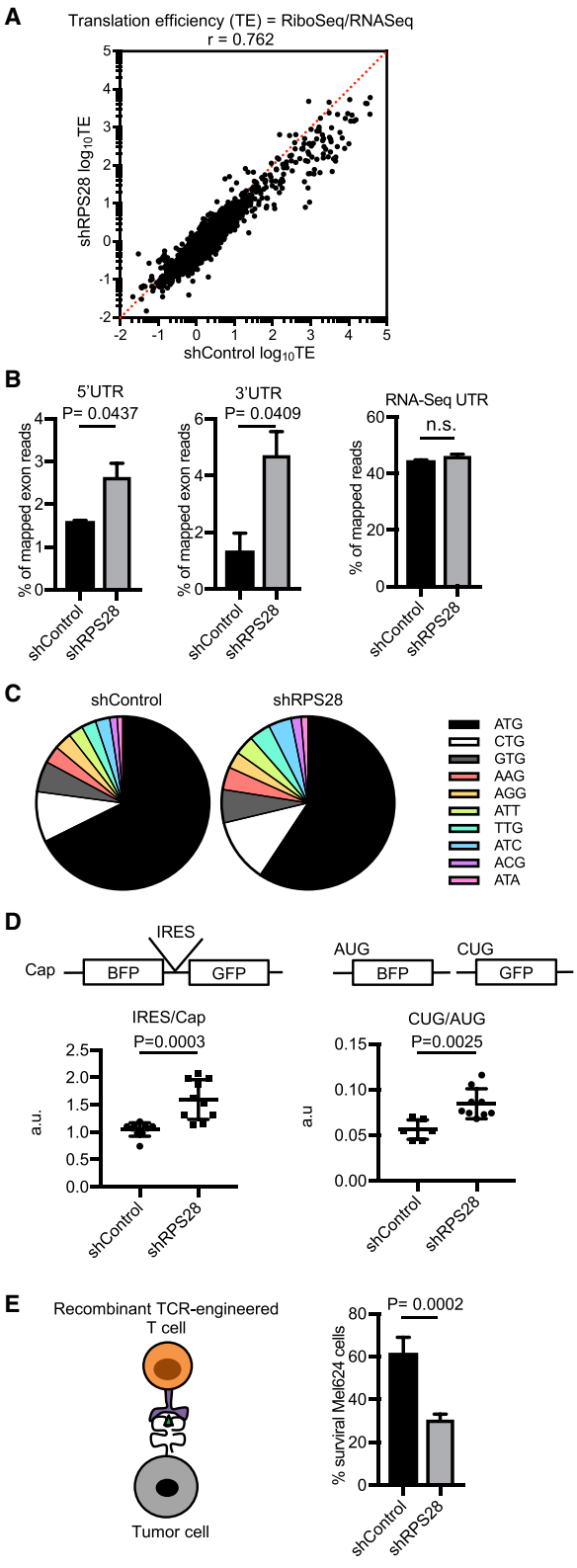

Figure 6. RPS28 Regulates Non-canonical Translation and Modulates Tumor Immunosurveillance

(A) Correlation of translation efficiencies of shControl and RPS28 knockdown.

chaperones) increasing access of nascent polypeptides to TAP/ER translocon with or without proteasome degradation.

Remarkably, RPL28 contacts RPL6, which when knocked down exerts the opposite effect in reducing antigenic peptide generation from IAV proteins, but, intriguingly, only those that are generated in a Ub E1-dependent manner. Since RPL6 knockdown increases large molecular weight ubiquitylated substrates, our findings suggest that RPL6 is required for targeting ubiquitylated DRiPs to proteasomes adept at generating peptides for MHC class I immunosurveillance. The presence of RPL28 may decrease RPL6 function in targeting DRiP for class I peptide generation, accounting for the opposite effects of these RPs on peptide generation and their physical proximity.

RPS28 knockdown increases HLA-A2 cell-surface expression without changing total cellular expression of HLA-A2 itself or TAP. This, and the lack of effect on K^b expressed by the same cells points to an increased HLA-A2 peptide ligand supply. A ready explanation for this effect comes from Ribo-Seq and reporter assay analysis demonstrating a clear increase in non-canonical translation, a substantial fraction of which are probably DRiPs. The selectivity of A2 versus K^b is puzzling but well precedented by large differences in class I allomorph sensitivity to inhibiting E1 (Wei et al., 2017), proteasomes (Benham et al., 1998; Luckey et al., 2001; Vinitsky et al., 1997), TAP (Henderson et al., 1992; Smith and Lutz, 1996), and protein synthesis itself (Schubert et al., 2000).

We link RPS28 control of peptide generation to cancer immunosurveillance, suggesting that ribosome mutations, common in cancers (Vlachos, 2017), may be selected for immunoevasion from CD8+ T cells or NK cells. This raises the possibility of the ribosome as a druggable target in cancer immunotherapy, and potentially autoimmunity as well. While it is nearly inevitable that ribosome targeting therapeutics will have major side effects, these are likely to be tolerable relative to their clinical benefits, with proteasome inhibitor cancer therapy providing a clear example of the utility of even broader targeting of an essential cellular machine (Yong et al., 2018). Regardless of their natural roles in immunosurveillance, our findings establish that RPs can be individually targeted pharmacologically or genetically to modulate antigen presentation in various diseases.

(B) Percentages of reads mapped to 5′ UTR (left) and 3′ UTR (middle) among reads mapped to exons from Ribo-Seq and percentages of reads mapped to UTR from RNA-seq (right). Center values and error bars represent mean ± range. Statistical significance was evaluated with a one-tailed unpaired t test (n = 2 biological replicates). ns, non-significant.

(C) Analysis of start codons that initiate open reading frames with ORF-RATER score > 0.9.

(D) Reporter assays using BFP and GFP to compare cap-independent translation to cap-dependent translation (left) and CUG initiated translation to AUG-initiated translation (right). Statistical significance was evaluated with a two-tailed unpaired t test.

(E) Viability of lentiviral shRNA transduced Mel624 cells after co-culture with $CD8^+$ T cells. Center values and error bars represent mean ± SEM. Statistical significance was evaluated with a two-tailed unpaired t test (n = 3 biological replicates).

See also Figures S4 and S5.

STAR★METHODS

Detailed methods are provided in the online version of this paper and include the following:

- KEY RESOURCES TABLE
- CONTACT FOR REAGENT AND RESOURCE SHARING
- EXPERIMENTAL MODEL AND SUBJECT DETAILS
  - Cell culture
  - Cell line generation
  - Influenza A virus strains
  - Recombinant influenza A virus construction
- METHOD DETAILS
  - Lentiviral shRNAs
  - MHC-I peptide presentation screen and data analysis
  - RNA purification and microarray analysis
  - Proteomics, RiboMethSeq and statistical analysis
  - Class I peptide complex recovery
  - Ribo-Seq, RNA-Seq and Translation efficiency (TE)
  - Dual reporter assay
  - Immunoblotting
  - T cell and tumor cell co-culture assay
- QUANTIFICATION AND STATISTICAL ANALYSIS
- DATA AND SOFTWARE AVAILABILITY

SUPPLEMENTAL INFORMATION

Supplemental Information includes five figures and two tables and can be found with this article online at https://doi.org/10.1016/j.molcel.2018.12.020.

ACKNOWLEDGMENTS

We thank NIAID RTB Genomic Technologies for microarrays and the NCI CCR sequencing group for Ribo-seq and RNA-seq. We thank Pr. Y. Motorin (IMoPA UMR 7365 CNRS-UL) for bioinformatic analysis and interpreting the RiboMethSeq data. J.W., R.J.K., M.A., J.S.G., I.P.I., N.F., L.M.S., N.P.R., and J.W.Y. were supported by the Division of Intramural Research of the National Institutes of Health. S.-B.Q. was supported by the U.S. NIH (R01AG042400) and HHMI Faculty Scholar (55108556). N.D.-V., V. Marcel, A.V., F.C., and J.-J.D. were supported by Agence Nationale pour la Recherche (RIBOMETH ANR-13-BSV8-0012-01) and by the PAIR Sein program (ARC_INCa_LNCC_7625).

AUTHOR CONTRIBUTIONS

J.W. and J.W.Y. designed the study and wrote the manuscript. R.J.K. performed the T cell killing assay. M.A. and N.F. assisted in the Ribo-seq data analysis. C.S.C. developed the lentivirus set. N.D.-V., V. Marcel, A.V., F.C., S.F., L.A., V. Marchand, Y.C., and J.-J.D. carried out the quantitative MS and the RiboMethSeq assay. D.D. generated the ICP47 cell line, J.S.G. generated rIAVs, and I.P.I. assisted in the dual reporter assay. S.-B.Q., L.M.S., and N.P.R. contributed reagents and edited the manuscript. J.W.Y. supervised the study.

DECLARATION OF INTERESTS

The authors declare no competing interests.

Received: July 13, 2018
Revised: October 29, 2018
Accepted: December 21, 2018
Published: January 31, 2019

REFERENCES

Ajore, R., Raiser, D., McConkey, M., Jöud, M., Boidol, B., Mar, B., Saksena, G., Weinstock, D.M., Armstrong, S., Ellis, S.R., et al. (2017). Deletion of ribosomal protein genes is a common vulnerability in human cancer, especially in concert with *TP53* mutations. EMBO Mol. Med. *9*, 498–507.

Alksne, L.E., Anthony, R.A., Liebman, S.W., and Warner, J.R. (1993). An accuracy center in the ribosome conserved over 2 billion years. Proc. Natl. Acad. Sci. USA *90*, 9538–9541.

Anthony, R.A., and Liebman, S.W. (1995). Alterations in ribosomal protein RPS28 can diversely affect translational accuracy in Saccharomyces cerevisiae. Genetics *140*, 1247–1258.

Antón, L.C., and Yewdell, J.W. (2014). Translating DRiPs: MHC class I immunosurveillance of pathogens and tumors. J. Leukoc. Biol. *95*, 551–562.

Apcher, S., Daskalogianni, C., Lejeune, F., Manoury, B., Imhoos, G., Heslop, L., and Fåhraeus, R. (2011). Major source of antigenic peptides for the MHC class I pathway is produced during the pioneer round of mRNA translation. Proc. Natl. Acad. Sci. USA *108*, 11572–11577.

Apcher, S., Millot, G., Daskalogianni, C., Scherl, A., Manoury, B., and Fåhraeus, R. (2013). Translation of pre-spliced RNAs in the nuclear compartment generates peptides for the MHC class I pathway. Proc. Natl. Acad. Sci. USA *110*, 17951–17956.

Ayadi, L., Motorin, Y., and Marchand, V. (2018). Quantification of 2′-O-Me residues in RNA using next-generation sequencing (Illumina RiboMethSeq Protocol). Methods Mol. Biol. *1649*, 29–48.

Belin, S., Hacot, S., Daudignon, L., Therizols, G., Pourpe, S., Mertani, H.C., Rosa-Calatrava, M., and Diaz, J.J. (2010). Purification of ribosomes from human cell lines. Curr. Protoc. Cell Biol. *Chapter 3*. Unit 3.40.

Benham, A.M., Grommé, M., and Neefjes, J. (1998). Allelic differences in the relationship between proteasome activity and MHC class I peptide loading. J. Immunol. *161*, 83–89.

Berglund, P., Finzi, D., Bennink, J.R., and Yewdell, J.W. (2007). Viral alteration of cellular translational machinery increases defective ribosomal products. J. Virol. *81*, 7220–7229.

Bolger, A.M., Lohse, M., and Usadel, B. (2014). Trimmomatic: a flexible trimmer for Illumina sequence data. Bioinformatics *30*, 2114–2120.

Briggs, J.W., and Dinman, J.D. (2017). Subtractional heterogeneity: a crucial step toward defining specialized ribosomes. Mol. Cell *67*, 3–4.

Brooke, C.B., Ince, W.L., Wrammert, J., Ahmed, R., Wilson, P.C., Bennink, J.R., and Yewdell, J.W. (2013). Most influenza a virions fail to express at least one essential viral protein. J. Virol. *87*, 3155–3162.

Bullock, T.N.J., and Eisenlohr, L.C. (1996). Ribosomal scanning past the primary initiation codon as a mechanism for expression of CTL epitopes encoded in alternative reading frames. J. Exp. Med. *184*, 1319–1329.

Coulie, P.G., Lehmann, F., Lethé, B., Herman, J., Lurquin, C., Andrawiss, M., and Boon, T. (1995). A mutated intron sequence codes for an antigenic peptide recognized by cytolytic T lymphocytes on a human melanoma. Proc. Natl. Acad. Sci. USA *92*, 7976–7980.

Cox, J., and Mann, M. (2008). MaxQuant enables high peptide identification rates, individualized p.p.b.-range mass accuracies and proteome-wide protein quantification. Nat. Biotechnol. *26*, 1367–1372.

Croft, N.P., Smith, S.A., Wong, Y.C., Tan, C.T., Dudek, N.L., Flesch, I.E., Lin, L.C., Tscharke, D.C., and Purcell, A.W. (2013). Kinetics of antigen expression and epitope presentation during virus infection. PLoS Pathog. *9*, e1003129.

Dinman, J.D. (2016). Pathways to specialized ribosomes: the Brussels lecture. J. Mol. Biol. *428* (10 Pt B), 2186–2194.

Dolan, B.P., Knowlton, J.J., David, A., Bennink, J.R., and Yewdell, J.W. (2010a). RNA polymerase II inhibitors dissociate antigenic peptide generation from normal viral protein synthesis: a role for nuclear translation in defective ribosomal product synthesis? J. Immunol. *185*, 6728–6733.

Dolan, B.P., Li, L., Takeda, K., Bennink, J.R., and Yewdell, J.W. (2010b). Defective ribosomal products are the major source of antigenic peptides

endogenously generated from influenza A virus neuraminidase. J. Immunol. *184*, 1419–1424.

Dunn, J.G., and Weissman, J.S. (2016). Plastid: nucleotide-resolution analysis of next-generation sequencing and genomics data. BMC Genomics *17*, 958.

Erales, J., Marchand, V., Panthu, B., Gillot, S., Belin, S., Ghayad, S.E., Garcia, M., Laforêts, F., Marcel, V., Baudin-Baillieu, A., et al. (2017). Evidence for rRNA 2′-O-methylation plasticity: control of intrinsic translational capabilities of human ribosomes. Proc. Natl. Acad. Sci. USA *114*, 12934–12939.

Esquivel, F., Yewdell, J., and Bennink, J. (1992). RMA/S cells present endogenously synthesized cytosolic proteins to class I-restricted cytotoxic T lymphocytes. J. Exp. Med. *175*, 163–168.

Fields, A.P., Rodriguez, E.H., Jovanovic, M., Stern-Ginossar, N., Haas, B.J., Mertins, P., Raychowdhury, R., Hacohen, N., Carr, S.A., Ingolia, N.T., et al. (2015). A regression-based analysis of ribosome-profiling data reveals a conserved complexity to mammalian translation. Mol. Cell *60*, 816–827.

Henderson, R.A., Michel, H., Sakaguchi, K., Shabanowitz, J., Appella, E., Hunt, D.F., and Engelhard, V.H. (1992). HLA-A2.1-associated peptides from a mutant cell line: a second pathway of antigen presentation. Science *255*, 1264–1266.

Higgins, R., Gendron, J.M., Rising, L., Mak, R., Webb, K., Kaiser, S.E., Zuzow, N., Riviere, P., Yang, B., Fenech, E., et al. (2015). The unfolded protein response triggers site-specific regulatory ubiquitylation of 40S ribosomal proteins. Mol. Cell *59*, 35–49.

Hill, A., Jugovic, P., York, I., Russ, G., Bennink, J., Yewdell, J., Ploegh, H., and Johnson, D. (1995). Herpes simplex virus turns off the TAP to evade host immunity. Nature *375*, 411–415.

Huang, W., Sherman, B.T., and Lempicki, R.A. (2009). Systematic and integrative analysis of large gene lists using DAVID bioinformatics resources. Nat. Protoc. *4*, 44–57.

Ingolia, N.T., Lareau, L.F., and Weissman, J.S. (2011). Ribosome profiling of mouse embryonic stem cells reveals the complexity and dynamics of mammalian proteomes. Cell *147*, 789–802.

Ingolia, N.T., Brar, G.A., Rouskin, S., McGeachy, A.M., and Weissman, J.S. (2012). The ribosome profiling strategy for monitoring translation in vivo by deep sequencing of ribosome-protected mRNA fragments. Nat. Protoc. *7*, 1534–1550.

Joyce, S., Kuzushima, K., Kepecs, G., Angeletti, R.H., and Nathenson, S.G. (1994). Characterization of an incompletely assembled major histocompatibility class I molecule (H-2Kb) associated with unusually long peptides: implications for antigen processing and presentation. Proc. Natl. Acad. Sci. USA *91*, 4145–4149.

Kandoth, C., McLellan, M.D., Vandin, F., Ye, K., Niu, B., Lu, C., Xie, M., Zhang, Q., McMichael, J.F., Wyczalkowski, M.A., et al. (2013). Mutational landscape and significance across 12 major cancer types. Nature *502*, 333–339.

Kim, W., Bennett, E.J., Huttlin, E.L., Guo, A., Li, J., Possemato, A., Sowa, M.E., Rad, R., Rush, J., Comb, M.J., et al. (2011). Systematic and quantitative assessment of the ubiquitin-modified proteome. Mol. Cell *44*, 325–340.

Kowarz, E., Löscher, D., and Marschalek, R. (2015). Optimized Sleeping Beauty transposons rapidly generate stable transgenic cell lines. Biotechnol. J. *10*, 647–653.

Langmead, B., Trapnell, C., Pop, M., and Salzberg, S.L. (2009). Ultrafast and memory-efficient alignment of short DNA sequences to the human genome. Genome Biol. *10*, R25.

Lee, A.S., Burdeinick-Kerr, R., and Whelan, S.P. (2013). A ribosome-specialized translation initiation pathway is required for cap-dependent translation of vesicular stomatitis virus mRNAs. Proc. Natl. Acad. Sci. USA *110*, 324–329.

Love, M.I., Huber, W., and Anders, S. (2014). Moderated estimation of fold change and dispersion for RNA-seq data with DESeq2. Genome Biol. *15*, 550.

Luckey, C.J., Marto, J.A., Partridge, M., Hall, E., White, F.M., Lippolis, J.D., Shabanowitz, J., Hunt, D.F., and Engelhard, V.H. (2001). Differences in the expression of human class I MHC alleles and their associated peptides in the presence of proteasome inhibitors. J. Immunol. *167*, 1212–1221.

Marchand, V., Blanloeil-Oillo, F., Helm, M., and Motorin, Y. (2016). Illumina-based RiboMethSeq approach for mapping of 2′-O-Me residues in RNA. Nucleic Acids Res. *44*, e135.

Mátés, L., Chuah, M.K., Belay, E., Jerchow, B., Manoj, N., Acosta-Sanchez, A., Grzela, D.P., Schmitt, A., Becker, K., Matrai, J., et al. (2009). Molecular evolution of a novel hyperactive Sleeping Beauty transposase enables robust stable gene transfer in vertebrates. Nat. Genet. *41*, 753–761.

McGlincy, N.J., and Ingolia, N.T. (2017). Transcriptome-wide measurement of translation by ribosome profiling. Methods *126*, 112–129.

Patel, S.J., Sanjana, N.E., Kishton, R.J., Eidizadeh, A., Vodnala, S.K., Cam, M., Gartner, J.J., Jia, L., Steinberg, S.M., Yamamoto, T.N., et al. (2017). Identification of essential genes for cancer immunotherapy. Nature *548*, 537–542.

Porgador, A., Yewdell, J.W., Deng, Y., Bennink, J.R., and Germain, R.N. (1997). Localization, quantitation, and in situ detection of specific peptide-MHC class I complexes using a monoclonal antibody. Immunity *6*, 715–726.

Prasad, S., Starck, S.R., and Shastri, N. (2016). Presentation of cryptic peptides by MHC class I is enhanced by inflammatory stimuli. J. Immunol. *197*, 2981–2991.

Quinlivan, M., Zamarin, D., García-Sastre, A., Cullinane, A., Chambers, T., and Palese, P. (2005). Attenuation of equine influenza viruses through truncations of the NS1 protein. J. Virol. *79*, 8431–8439.

Schmidt, A. (2009). Nonsense Mediated Decay Associated Pioneer Round of Translation as Source for Peptides for Presentation by MHC Class I (University of Koln).

Schubert, U., Antón, L.C., Gibbs, J., Norbury, C.C., Yewdell, J.W., and Bennink, J.R. (2000). Rapid degradation of a large fraction of newly synthesized proteins by proteasomes. Nature *404*, 770–774.

Schwanhäusser, B., Busse, D., Li, N., Dittmar, G., Schuchhardt, J., Wolf, J., Chen, W., and Selbach, M. (2011). Global quantification of mammalian gene expression control. Nature *473*, 337–342.

Shi, Z., and Barna, M. (2015). Translating the genome in time and space: specialized ribosomes, RNA regulons, and RNA-binding proteins. Annu. Rev. Cell Dev. Biol. *31*, 31–54.

Shi, Z., Fujii, K., Kovary, K.M., Genuth, N.R., Rost, H.L., Teruel, M.N., and Barna, M. (2017). Heterogeneous ribosomes preferentially translate distinct subpools of mRNAs genome-wide. Mol. Cell *67*, 71–83.e77.

Smith, K.D., and Lutz, C.T. (1996). Peptide-dependent expression of HLA-B7 on antigen processing-deficient T2 cells. J. Immunol. *156*, 3755–3764.

Starck, S.R., and Shastri, N. (2016). Nowhere to hide: unconventional translation yields cryptic peptides for immune surveillance. Immunol. Rev. *272*, 8–16.

Starck, S.R., Jiang, V., Pavon-Eternod, M., Prasad, S., McCarthy, B., Pan, T., and Shastri, N. (2012). Leucine-tRNA initiates at CUG start codons for protein synthesis and presentation by MHC class I. Science *336*, 1719–1723.

Trapnell, C., Pachter, L., and Salzberg, S.L. (2009). TopHat: discovering splice junctions with RNA-Seq. Bioinformatics *25*, 1105–1111.

Tscharke, D.C., Karupiah, G., Zhou, J., Palmore, T., Irvine, K.R., Haeryfar, S.M., Williams, S., Sidney, J., Sette, A., Bennink, J.R., and Yewdell, J.W. (2005). Identification of poxvirus CD8+ T cell determinants to enable rational design and characterization of smallpox vaccines. J. Exp. Med. *201*, 95–104.

Vinitsky, A., Anton, L.C., Snyder, H.L., Orlowski, M., Bennink, J.R., and Yewdell, J.W. (1997). The generation of MHC class I-associated peptides is only partially inhibited by proteasome inhibitors: involvement of nonproteasomal cytosolic proteases in antigen processing? J. Immunol. *159*, 554–564.

Vlachos, A. (2017). Acquired ribosomopathies in leukemia and solid tumors. Hematology (Am. Soc. Hematol. Educ. Program) *2017*, 716–719.

Wang, F., Durfee, L.A., and Huibregtse, J.M. (2013). A cotranslational ubiquitination pathway for quality control of misfolded proteins. Mol. Cell *50*, 368–378.

Wei, J., Gibbs, J.S., Hickman, H.D., Cush, S.S., Bennink, J.R., and Yewdell, J.W. (2015). Ubiquitous autofragmentation of fluorescent proteins creates

abundant defective ribosomal products (DRiPs) for immunosurveillance. J. Biol. Chem. *290*, 16431–16439.

Wei, J., Zanker, D., Di Carluccio, A.R., Smelkinson, M.G., Takeda, K., Seedhom, M.O., Dersh, D., Gibbs, J.S., Yang, N., Jadhav, A., et al. (2017). Varied role of ubiquitylation in generating MHC class I peptide ligands. J. Immunol. *198*, 3835–3845.

Wieczorek, S., Combes, F., Lazar, C., Giai Gianetto, Q., Gatto, L., Dorffer, A., Hesse, A.M., Couté, Y., Ferro, M., Bruley, C., and Burger, T. (2017). DAPAR & ProStaR: software to perform statistical analyses in quantitative discovery proteomics. Bioinformatics *33*, 135–136.

Xue, S., and Barna, M. (2012). Specialized ribosomes: a new frontier in gene regulation and organismal biology. Nat. Rev. Mol. Cell Biol. *13*, 355–369.

Yang, N., Gibbs, J.S., Hickman, H.D., Reynoso, G.V., Ghosh, A.K., Bennink, J.R., and Yewdell, J.W. (2016). Defining viral defective ribosomal products: standard and alternative translation initiation events generate a common peptide from influenza A virus M2 and M1 mRNAs. J. Immunol. *196*, 3608–3617.

Yewdell, J.W., and Nicchitta, C.V. (2006). The DRiP hypothesis decennial: support, controversy, refinement and extension. Trends Immunol. *27*, 368–373.

Yewdell, J.W., Anton, L.C., and Bennink, J.R. (1996). Defective ribosomal products (DRiPs): a major source of antigenic peptides for MHC class I molecules? J. Immunol. *157*, 1823–1826.

Yong, K., Gonzalez-McQuire, S., Szabo, Z., Schoen, P., and Hajek, R. (2018). The start of a new wave: developments in proteasome inhibition in multiple myeloma. Eur. J. Haematol. Published online March 30, 2018. https://doi.org/10.1111/ejh.13071.

STAR★METHODS

KEY RESOURCES TABLE

REAGENT or RESOURCE	SOURCE	IDENTIFIER
Antibodies		
Mouse anti-HLA-A,B,C (clone W6/32)	In house/ATCC	ATCC HB-95
Mouse anti-H-2K^b (HB176)	In house/ATCC	ATCC HB-176
Mouse anti-b2m (clone BBM.1)	In house/ATCC	ATCC HB-28
Mouse anti-HLA-A2 (clone MA2.1)	In house/ATCC	ATCC HB-54
Mouse anti-NA (clone NA2-1C1)	Brooke et al., 2013	N/A
Mouse anti-M2 (clone M2-1C6)	Brooke et al., 2013	N/A
Mouse anti-K^b-SIINFKEL (clone 25D1.16)	Porgador et al., 1997	N/A
Mouse anti-CD8 (3B5)	ThermoFisher	MHCD0801
Mouse anti-IFN-γ (clone XMG1.2)	eBioscience	Cat# 17-7311-81
Rabbit anti-histone H3 (clone D1H2)	Cell Signaling Technology	Cat# 4499; RRID: AB_10544537
Mouse anti-GAPDH (clone 1E6D9)	proteintech	Cat# 60004-1-Ig; RRID: AB_2107436
Mouse anti-mono and polyubiquitin Ab (clone FK2)	Enzo Life Sciences	Cat# BML-PW8810; RRID: AB_10541840
Rabbit anti-RPS28	Abcam	Cat# ab133963
Rabbit anti-RPL28	Abcam	Cat# ab138125
Rabbit anti-RPL6	Abcam	Cat# ab126100
Mouse anti-HLA class I ABC	Abcam	Cat# ab70328
Mouse anti-TAP1 (clone 148.3)	Millipore Sigma	Cat# MABF125
Rabbit anti-H2K^b (exon8)	Joyce et al., 1994	N/A
IRDye 800CW goat anti-rabbit IgG (H+L)	LI-COR	Cat# P/N 925-32211
IRDye 680LT goat anti-mouse IgG (H+L)	LI-COR	Cat# P/N 925-68020
Alexa Fluor 647–coupled goat anti-mouse IgG (H+L)	Thermo Fisher	Cat# A28181
Bacterial and Virus Strains		
rIAV-NA-SIINFEKL	Dolan et al., 2010b	N/A
rIAV-M2(C-term)-SIINFEKL	Yang et al., 2016	N/A
rIAV-NS1-SIINFEKL	This paper	N/A
rIAV-M2(45)-SIINFEKL	Yang et al., 2016	N/A
rIAV-Ub-SIINFEKL	This paper	N/A
rIAV-ES-SIINFEKL	This paper	N/A
Chemicals, Peptides, and Recombinant Proteins		
Puromycin dihydrochloride	Sigma-Aldrich	Cat# P9620-10ML
Cycloheximide	Sigma-Aldrich	Cat# C7698
MLN7243	National Centre for Advancing Translational Sciences	N/A
BFA	Sigma-Aldrich	Cat # B5936
Critical Commercial Assays		
Ribo-Zero Gold rRNA removal Kit (Human, Mouse, Rat)	Illumina	Cat# MRZG12324
SMARTer total RNA Pico kit	Clontech	Cat# 634411
Deposited Data		
Raw and analyzed microarray data	This paper	GEO: GSE114484
Experimental Models: Cell Lines		
Human: Mel624 cells	Patel et al., 2017	N/A
Human: Hek293-K^b	Tscharke et al., 2005	N/A
Human: Hek293-K^b-ICP47	This paper	N/A

(*Continued on next page*)

Continued		
REAGENT or RESOURCE	SOURCE	IDENTIFIER
Human: Hek293-K^b-Control-ICP47	This paper	N/A
Human: T cells transduced with recognizing the HLA-A*02-restricted melanoma antigens NY-ESO-1	Patient derived; Patel et al., 2017	N/A
Human: Lenti-X 293T	Clontech	Cat# 632180
Experimental Models: Organisms/Strains		
Mouse: OT-I: C57BL/6-Tg(TcraTcrb)1100Mjb/J	The Jackson Laboratory	Cat# 003831
Oligonucleotides		
shRNA targeting sequence	This paper	N/A
Recombinant DNA		
pDZ	Quinlivan et al., 2005	N/A
pSBbi-Pur	Kowarz et al., 2015	Addgene Plasmid #60523
pCMV(CAT)T7-SB100	Mátés et al., 2009	Addgene plasmid #34879
pTagBFP-N	evrogen	Cat# FP172
pIRES2-EGFP	Clontech	Cat# 6029-1
pEGFP-N1	Clontech	Cat# 6085-1
Software and Algorithms		
Visualization and Integrated Discovery (DAVID) v6.8	Huang et al., 2009	https://david.ncifcrf.gov
MaxQuant	Cox and Mann, 2008	https://www.biochem.mpg.de/5111795/maxquant
ProStaR	Wieczorek et al., 2017	https://bioconductor.org/packages/release/bioc/html/Prostar.html
Bowtie	Langmead et al., 2009	http://bowtie-bio.sourceforge.net/index.shtml
Tophat	Trapnell et al., 2009	https://ccb.jhu.edu/software/tophat/index.shtml
Plastid	Dunn and Weissman, 2016	https://plastid.readthedocs.io/en/latest/
ORF-RATER	Fields et al., 2015	https://github.com/alexfields/ORF-RATER
Trimmomatic	Bolger et al., 2014	http://www.usadellab.org/cms/?page=trimmomatic
DESeq2	Love et al., 2014	https://bioconductor.org/packages/release/bioc/html/DESeq2.html

CONTACT FOR REAGENT AND RESOURCE SHARING

Further information and requests for resources and reagents should be directed to and will be fulfilled by the Lead Contact, Jonathan W. Yewdell (jyewdell@niaid.nih.gov).

EXPERIMENTAL MODEL AND SUBJECT DETAILS

Cell culture

HEK293-K^b, Mel624, Lenti-X 293T, and HEK293-K^b-ICP47 and the corresponding control cells were maintained in Dulbecco's Modified Eagle's Medium (DMEM) with 10% fetal bovine serum (FBS). All cultures were grown at 37°C in a 5% CO2 incubator and tested to be free of mycoplasma contamination. Human T cells transduced with recognizing the HLA-A*02-restricted melanoma antigens NY-ESO-1 were cultured in T cell medium: AIM-V medium supplemented with 5% human AB serum, 100 U ml^{-1} penicillin and 100 μg ml^{-1} streptomycin, 2 mM L-glutamine and 12.5 mM HEPES.

Cell line generation

For HEK293-K^b-ICP47 cells generation, a bacterial artificial chromosome with the herpes simplex virus type 1 genome was a generous gift of David Leib (Dartmouth) and Thomas Kristie (NIAID, NIH). The ICP47 gene was amplified with the following primers: 5′-TAGAAGGCCTCTGAGGCCATGTCGTGGGCCCTGGAAATGGCG-3′, 5′-TTGATGGCCTGACAGGCCTCAACGGGTTACCGGAT TACGGGG-3′ and cloned into the SfiI site of the pSBbi-Pur Sleeping Beauty expression vector (a gift from Eric Kowarz, Addgene plasmid #60523). HEK293-K^b cells were transfected with either the base pSBbi-Pur vector or the ICP47 pSBbi-Pur vector along with 1/20 amount of Sleeping Beauty 100x (a gift from Zsuzsanna Izsvak, Addgene plasmid #34879). Transfected cells were selected in 2 μg ml^{-1} puromycin to generate a stable population.

Influenza A virus strains

Recombinant Influenza A virus A/Puerto Rico/8/34 (rIAVs) expressing SIINFEKL were described previously (Dolan et al., 2010b; Yang et al., 2016) or below. rIAVs was grown in 10-d embryonic chicken eggs and used as infectious allantoic fluid.

Recombinant influenza A virus construction

PB1-ES-SIINFEKL was cloned as a three-segment assembly using NEBuilder HiFi DNA Assembly Master Mix (New England Biolabs) with vector pDZ digested with restriction enzyme SapI. The left half consisted of all of the PB1 segment up to the end of the PB1 coding sequence PCR amplified with the universal influenza primer IAV 5′ SapI 5′-AGCTCTTCAGGGAGCAAAAGCAGG-3′ and primer PB1 AgeI bot 5′-TTTCACCGGTGCTTTTTGCCGTCTGAGCTCTTCAATG-3′. The right half consisted of FMV 2A-ES-SIINFEKL fused to the final 270bp of PB1 as follows. The final 270bp of the PB1 segment was PCR amplified with primers ES-SIIN-PB1 top 5′-GCGGCAGTCTGCAGCGCGGCCAGTATAATCAACTTTGAAAAACTGTAGTTGAAGATGAACAAATGTACC-3′ and universal flu primer IAV 3′ SapI 5′-TGCTCTTCTATTAGTAGAAACAAGG-3′, extended by PCR amplification with primers 2A-ES-SIIN top 5′-TGAGTCCAACCCTGGGCCCATGAGGTACATGATTTTAGGCTTGCTCGCCCTTGCGGCAGTCTGCAGCGCGGCCAG-3′ and IAV 3′ SapI to add ES signal sequence, followed by further extension by PCR amplification with primers ES-SIIN-PB1 AgeI top 5′-AGCACCGGTGAAACAGACTTTGAATTTTGACCTTCTCAAGTTGGCAGGAGACGTTGAGTCCAACCCTGGGCCCATG-3′ and IAV 3′ SapI to add the 24-mer FMV 2A sequence. PCR products were purified by agarose gel electrophoresis and QIAquick spin cartridges (QIAGEN) between each step. Final PCR products were digested with SapI (pDZ vector), or SapI and AgeI (left and right insert fragments) and heat inactivated prior to assembly.

PB1-Ub-SIINFEKL was cloned in a manner similar to PB1-ES-SIINFEKL except that the right insert fragment was replaced with FMV 2A fused to Ubiquitin-SIINFEKL- and the final 270bp of PB1. The final 270bp of the PB1 segment was PCR amplified as above with primers SIIN-PB1 top 5′-ATAATCAACTTTGAAAAACTGTAGTTGAAGATGAACAAATGTAC-3′ and universal flu primer IAV 3′ SapI. Ubiquitin was PCR amplified with primers 2A-Ub-top 5′-GACCTTCTCAAGTTGGCAGGAGACGTTGAGTCCAACCCTGGGC CCATGCAGATCTTCGTGAAGAC-3′ and Ub-SIIN bot 5′-ACAGTTTTTCAAAGTTGATTATACTACCACCTCTTAGTCTTAAGAC-3′. The PCR products of Ubiquitin and the final 270bp of PB1 were joined via splice overlap extension, while simultaneously adding the 24-mer FMV 2A sequence using primers 2A AgeI top 5′-AGCACCGGTGAAACAGACTTTGAATTTTGACCTTCTCAAGTTGG-3′ and IAV 3′ SapI. Final PCR products were digested with SapI (pDZ vector) or SapI and AgeI as above (left and right insert fragments) prior to assembly.

The NS1-SIINFEKL plasmid was generated by mutagenesis of plasmid pDZ-PR8-NS1 using primers NS1-SIIN top 5′-ACGG CCTCTCGATCTATCGCTACTACGGCTTGTCGATCATCAACTTCGAGAAGCTCTACCTAACTGACATGACTCTTGAG-3′ and NS1-SIIN bot 5′-AGCGATAGATCGAGAGGCCGTAGTACCTGTAAATACTCAGCCCGTAGTAACGATAAATACTACGCGACGCAGGTAC AGAG-3′ using QuikChange II site directed mutagenesis kit (Agilent).

METHOD DETAILS

Lentiviral shRNAs

All shRNA targeting sequences were cloned into DECIPHER pRSI9-U6- (sh)-UbiC-TagRFP-2A-Puro (Cellecta, CA). shRNA targeting sequences listed in Table S1 were based on RNAi consortium at Broad Institute (https://portals.broadinstitute.org/gpp/public/). Lentiviral particles were packaged using Lenti-X 293T cells (Clontech) according to the manufacturer's instructions. Virus-containing supernatants were collected at 48-h after transfection and filtered to eliminate cell contaminates. Target cells were infected by shRNA lentivirus in 5 μg ml^{-1} polybrene at MOI = 2 to achieve approximately 50% transduction efficiency for flow cytometry assay that differentiates cells by RFP signal, and at MOI = 5 for other assays.

MHC-I peptide presentation screen and data analysis

For steady state Class I, cells infected with shRNA lentivirus were stained with fluorochrome-conjugated Abs including anti-HLA-A,B,C (W6/32, prepared in-house), anti-H-2K^b (HB176, prepared in-house), anti-β2 m (BBM.1, prepared in-house), and anti-HLA-A2 (MA2.1, prepared in-house). For SIINFEKL presentation, cells infected with shRNA lentivirus were resuspended in FBS-free acidified RPMI 1640 medium, infected with rIAV at MOI = 10 at 37°C, resuspended in culture medium, harvested at indicated time points, and stained with fluorochrome-conjugated Abs including anti-NA (NA2-1C1, prepared in-house), anti-M2 (M2-1C6, prepared in-house) and anti-K^b-SIINFEKL (25D1.16, prepared in-house). ES and Ub were UV inactivated before use to avoid saturation of K^b-SIINFEKL on cell surface. Fluorochrome conjugation using antibody labeling kit (ThermoFisher) was conducted following manufacturer's instructions. Secondary staining was conducted with Alexa Fluor 647–coupled goat anti-mouse IgG (H+L) (Life Technologies), when necessary. Flow cytometric data were acquired using a BD LSR Fortessa X-20 flow cytometer (BD Biosciences), gated on single cells, and data were analyzed with FlowJo version 9.8.5 software (FlowJo LLC).

RNA purification and microarray analysis

6 days after lentivirus transduction, total RNA was isolated from 1 × 10^6 cells by TRIzol reagent (Invitrogen), purified by RNeasy Mini Kit and analyzed by HumanHT-12 Gene Expression BeadChip (Illumina) at NIAID Research Technologies Branch. Raw data were analyzed by JMP/Genomics software 7.0 with SAS Version 9.4 to calculate lsmeans, $\log_2$ (fold change), negative $\log_{10}$ (p value),

and determine statistical significance. lsmeans were used to plot heatmap in Figure 2A with the Python function seaborn.heatmap. log_2 (fold change) and negative log_{10} (p value) were used to generate volcano plots in Figures 2 and S2 by R package ggplots. Significant changed genes were analyzed by Visualization and Integrated Discovery (DAVID) v6 0.8 (NIAID) for Gene Ontology (GO) terms enrichment to generate Figure 2D.

Proteomics, RiboMethSeq and statistical analysis

Five replicates of ribosomes were purified as described (Belin et al., 2010) before characterization by MS-based proteomic analysis as described (Erales et al., 2017). Briefly, extracted proteins were stacked in the top of a 4%–12% NuPAGE gel (Invitrogen) before in-gel digestion using modified trypsin (Promega). Resulting peptides were analyzed by nanoliquid chromatography coupled to tandem MS (Ultimate 3000 RSLCnano system coupled to Q-Exactive Plus, Thermo Scientific) using a 120-min gradient. RAW files were processed using MaxQuant (Cox and Mann, 2008) version 1.5.8.3 and the SwissProt database (*Homo sapiens* taxonomy, June 2017 version). Intensity-based absolute quantification (iBAQ) (Schwanhäusser et al., 2011) values were calculated from MS intensities of unique and razor peptides and used for statistical analyses using ProStaR (Wieczorek et al., 2017). Only proteins quantified in at least 5 replicates of 1 condition were kept. For each sample, individual iBAQ values were normalized by the sum of iBAQ values extracted from ribosomal proteins. Missing data were imputed using the 0.5-percentile value of each column before statistical testing using *limma* t test. Differentially expressed proteins were sorted out using a log_2 (fold change) cut-off of 1 and an adjusted p value allowing to reach a FDR threshold below 0.5% using the Benjamini-Hochberg method. Site-specific rRNA methylation was determined by RiboMethSeq, as previously described (Marchand et al., 2016). Briefly 150 ng of total RNA were subjected to alkaline hydrolysis for 14 min at 96°C followed by end-repair and library preparation using NEBNext Small RNA Library kit (NEB, UK) following the manufacturer's instructions. Libraries were multiplexed and sequenced on Hiseq1000 at 6 pM. Bioinformatic analysis was performed as described (Ayadi et al., 2018).

Class I peptide complex recovery

Cells were treated with ice-cold citric acid buffer (0.13 M citric acid, 0.061 M Na_2HPO4, 0.15 M NaCl [pH 3]) at 1×10^7 cells ml^{-1} for 120 s, washed three times with PBS, and resuspended in culture medium. At the indicated time point, an aliquot of cells was removed and stained with Abs including anti-HLA-A,B,C (W6/32, prepared in-house) and anti-HLA-A2 (MA2.1, prepared in-house).

Ribo-Seq, RNA-Seq and Translation efficiency (TE)

Ribo-Seq experiments were conducted as described previously (McGlincy and Ingolia, 2017) with modification described below. Ribo-Zero Gold rRNA removal Kit (Human, Mouse, Rat) (Illumina) was used before reverse transcription. In addition to oligos described previously (Ingolia et al., 2012), oligos in Table S2 were also used to deplete rRNA. Ribo-Seq libraries were sequenced as SR 50 cycles on Illumina HiSeq 2000 instrument. Cutadapt was used to trim adaptor and select read lengths between 25 to 35 bp. After align to a pre-build rRNA library by Bowtie (Langmead et al., 2009), unaligned reads were then aligned to human genome hg19 by Tophat (Trapnell et al., 2009). Best alignment was analyzed by Plastid (Dunn and Weissman, 2016) to determine P-site offset. Gene position files containing only protein coding genes were built by Plastid. Reads were then tabulated as RPKM values and mapped to exon, CDS, 5′UTR, and 3′UTR by Plastid. Genes with CDS RPKM > 0.5 were kept for downstream analysis. RPKM values were used to plot Figures S4A and S5A. Best alignments were visualized by Integrative Genomics Viewer (IGV, Broad Institute) in Figure S4B. To identify open reading frames (ORFs), multiple alignments were kept, two replicates were merged and analyzed by ORF-RATER (Fields et al., 2015) to determine and rate ORFs. Start codons that initiate ORFs with rate score > 0.9 were shown in Figure 6C.

For RNA-Seq, total RNA was extracted by adding SDS (1% final concentration) to Ribo-Seq cell lysate and purified by RNA Clean & Concentrator (Zymo Research). RNA-Seq libraries were prepared by SMARTer total RNA Pico kit (Clontech) and sequenced as PE 75 cycles on Illumina NextSeq instrument. Trimmomatic (Bolger et al., 2014) was used for adaptor and quality filtering. Alignment to human genome hg19 was performed by TopHat. Reads were tabulated as RPKM values and mapped to exon, CDS, 5′UTR, and 3′UTR by Plastid. Genes with CDS RPKM > 0.5 were kept for downstream analysis.

Statistical analysis of differences in TE between shControl and shRPS28 was conducted using DESeq2. log_2 (fold change) and negative log_{10} (adjusted P value) were plotted in Figure S5B.

Dual reporter assay

To compare cap-dependent translation with cap-independent translation, BFP was amplified from pTagBFP-N (evrogen) using primers 5′-CAAGCTTCGAATTCTCGCCACCATGAGCGAGCTGAT-3′ and 5′-AGAGGGGCGGATCCCAGTCGCGGCCGCTTTAAT TAA-3′, digested with EcoRI and BamHI, and inserted into similarly digested pIRES2-EGFP. To compare AUG translation with CUG translation, GFP with start codon mutated to CTG and three CTG following start codon mutated to CTC or CTA was amplified from pEGFP-N1 using primers 5′- GATCCACCGGTCGCCACCAUGGTGAGCAAGGGCGAGGAGCTCTTCACCGGGGTGGTGCC CATCCTCGTCGAGCTAGACGGCGACGTA-3′ and 5′-TGATCTAGAGTCGCGGCCGCTTTACT-3′, digested with AgeI and XbaI, and inserted into similarly digested pEGFP-N1. Primers 5′-GGATCCACCGGTCGCCACCATGGTGAGCAAGGGCGA-3′ and 5′-TGAT CTAGAGTCGCGGCCGCTTTACT-3′ were then used to mutate start codon back to ATG. Transfection was conducted 5 days post

shRNA lentivirus infection, and GPF and BFP signal measured by flow cytometry 48-h post transfection. GFP and BFP plasmids were transfected individually in parallel to serve as single color controls and fluorescence minus one controls.

Immunoblotting

Whole cell lysates were generated as described previously (Wei et al., 2015). Blots were probed with rabbit anti-histone H3 (D1H2, Cell Signaling Technology), mouse anti-GAPDH (clone 1E6D9, proteintech), mouse anti-mono and polyubiquitin Ab (clone FK2; Enzo Life Sciences), rabbit anti-RPS28 (ab133963, Abcam), rabbit anti-RPL28 (ab138125, Abcam), rabbit anti-RPL6 (ab126100, Abcam), mouse anti-HLA Class I ABC (ab70328, Abcam), mouse anti-TAP1 (clone148.3, Millipore), followed by incubation with IRDye 800CW anti-rabbit Ab, and IRDye 680LT anti-mouse Ab (both from LI-COR). Protein was quantitated on an Odyssey infrared scanner using Image Studio v2.0 software (LI-COR)

T cell and tumor cell co-culture assay

T cell and tumor cell co-culture experiments were conducted as described previously (Patel et al., 2017). In short, NY-ESO-1 T cells used for co-culture assays were thawed and cultured in AIM-V medium (ThermoFisher) supplemented with 5% human AB serum (Valley Biomedical), 100U ml^{-1} penicillin and 100μg ml^{-1} streptomycin, 2mM L-glutamine, 12.5mM HEPES, and 300IU ml^{-1} IL-2. T cells were then co-cultured with RPS28 knockdown Mel624 cells at the effector:target ratio of 1:1 overnight. At the end of the co-culture, tumor cells were detached using trypsin and washed twice with PBS. Tumor cells and T cells were stained with fixable Live/Dead dye (ThermoFisher) followed by human anti-CD3 antibody (clone SK7, BioLegend). Live, CD3- cell counts were measured by CountBright Absolute Counting Beads (ThermoFisher).

QUANTIFICATION AND STATISTICAL ANALYSIS

The type of statistical test is annotated in the Figure legend and/or in the Method Details section specific to the analysis. In addition, statistical parameters such as the value of n, mean/median, SEM, SD and significance level are reported in the Figures and/or in the Figure Legends. A P value less than or equal to 0.05 was considered statistically significant for all analyses unless indicated otherwise. Prism (GraphPad Software Inc.) was used for these analyses unless indicated otherwise.

DATA AND SOFTWARE AVAILABILITY

The microarray data have been deposited in the Gene Expression Omnibus database under accession number GEO: GSE114484.